Influence of the Impregnation pH on the Surface Characteristics and the Catalytic Activity of the Mo/γ-Al_2O_3 and CoMo/γ-Al_2O_3 Hydrodesulfurization Catalysts Prepared by Equilibrium Deposition Filtration (EDF)

J. Vakros, K. Bourikas, Ch. Kordulis, and A. Lycourghiotis*

Department of Chemistry, University of Patras, GR-265 00, Patras, Greece, and Institute of Chemical Engineering & High-Temperature Chemical Processes (ICE/HT), P.O. Box 1414, GR-265 00, Patras, Greece

Received: April 10, 2002; In Final Form: October 3, 2002

Two unpromoted Mo/γ-Al_2O_3 catalysts containing almost the same amount of Mo were prepared using equilibrium deposition filtration, EDF, for depositing Mo-oxo species on the alumina surface at two different pH values (3.9 and 6.3). On these samples the same amount of Co ions was deposited by dry impregnation and thus, the corresponding CoMo/γ-Al_2O_3 catalysts were prepared. The unpromoted and the Co-promoted samples were characterized using BET, DRS, LRS, TPR, and NO chemisorption. Moreover, the catalytic activity of the samples was determined at various temperatures using the hydrodesulfurization of thiophene as a probe reaction. The characterization of the specimens showed that the Mo deposition at pH = 3.9 favors the deposition of polymeric Mo-oxo species, in agreement with predictions drawn on the basis of two models related with the acid−base behavior of the γ-Al_2O_3 surface. These species after calcination provide a well-dispersed Mo phase with relatively high reducibility. This phase, in which the concentration of the octahedral Mo is greater compared to that on the Mo/γ-Al_2O_3 specimen prepared at pH = 6.3, hinders, in turn, the formation of the catalytically inactive $CoAl_2O_4$, whereas after sulfidation this provides a sulfided state with relatively high concentration of sulfur vacancies. The above explain why the unpromoted and the Co-promoted catalysts prepared at pH = 3.9 proved to be more active than the corresponding catalysts prepared at pH = 6.3.

Introduction

It is well-known that the preparation of the (Co or Ni)Mo/γ-Al_2O_3 sulfided catalysts used in oil hydrodesulfurization is quite complicated, involving several steps (deposition of Mo-oxo species on the γ-alumina surface followed by drying and air-calcination as well as deposition of the $Co(H_2O)_6^{2+}$ or $Ni(H_2O)_6^{2+}$ species on the precursor Mo/γ-Al_2O_3 solid followed by drying, calcination, and finally in situ sulfidation). The preparative parameters in each preparation step would be expected to have an influence on the structure and catalytic activity of the prepared catalysts. The deposition of the Mo-oxo species is the first and presumably quite critical preparation step. Much progress has been made in the past decades concerning the Mo species deposited or formed on the support surface during impregnation (e.g., refs 1−5). A plausible question raised is whether the Mo surface speciation achieved during deposition influences the structure of the oxidic and sulfided state and thus the catalytic activity. In other words, do the subsequent steps of preparation, mainly the high-temperature air-calcination and sulfidation procedures, bring about a complete disappearance of the differences in the Mo speciation obtained in the deposition step? To investigate this point and contribute to the preparation of the CoMo/γ-Al_2O_3 catalysts we have, in a previous paper, studied the influence of the preparation methodology on the physicochemical and catalytic properties of the CoMo/γ-Al_2O_3 catalysts prepared by five different methodologies.[6] In this work among others physicochemical parameters, we have studied the mode of the Mo deposition. It was found that the change of the methodology for depositing the Mo species (incipient wetness impregnation, wet impregnation, equilibrium deposition filtration, EDF, otherwise called equilibrium adsorption[7]) results in catalysts with different physicochemical properties and catalytic activity. Specifically, it was found that the most promising methodology involves the following steps: first, the deposition of the molybdenum oxo-species on the γ-Al_2O_3 surface through EDF followed by drying and air calcination; second, the deposition of the $Co(H_2O)_6^{2+}$ species on the Mo/γ-Al_2O_3 solid by pore volume impregnation followed by drying and air calcination, as well.

The amount of the Mo-oxo species deposited on the γ-Al_2O_3 surface using EDF increases with the Mo concentration in the impregnating solution, whereas it decreases with the impregnation pH. It is, therefore, possible to deposit on the support surface the *same amount* of the Mo-oxo species by selecting *different pairs of values* for the above-mentioned preparation parameters. On the other hand it has been well established that the deposited Mo surface species, following EDF, depend on the particular pair of the (pH, concentration) values selected to carry out the Mo deposition. It is, therefore, interesting to investigate whether the physicochemical characteristics of the Mo supported phase in the oxidic and sulfided state and thus the catalytic properties of the final CoMo/γ-Al_2O_3 catalysts are more or less related to the Mo species formed on the support surface during deposition performed at different (pH, concentration) pairs of values.

To investigate the above issue and with the underlying idea to develop further the methodology followed for preparing CoMo/γ-Al_2O_3 catalysts, we study in the present work two unpromoted and two Co-promoted samples containing almost

* Author to whom all correspondence should be addressed, Fax: (+30 2610) 994796. E-mail: kordulis@chemistry.upatras.gr.

10.1021/jp020953e CCC: $25.00
Published on Web 02/04/2003

the same amount of the supported Mo and Co. In the first (second) sample the deposition of the Mo using EDF has been taken place from a Mo solution with relatively low (high) Mo concentration and low (high) pH. The $Co(H_2O)_6^{2+}$ species has been deposited on the surface of the Mo/γ-Al_2O_3 precursor solids by pore volume impregnation.

The above unpromoted and Co-promoted samples were characterized, using BET, NO adsorption, temperature-programmed reduction (TPR), laser Raman spectroscopy (LRS), and UV−Vis diffuse reflectance spectroscopy (DRS). Moreover, the catalytic activity of the prepared samples was determined using the hydrodesulfurization of thiophene as a probe reaction. An interpretation of the catalytic results in terms of the physicochemical properties of the catalysts studied is also attempted.

Experimental Section

Preparation of the Samples. The construction of the adsorption isotherms related to the deposition of the Mo-oxo species on the γ-Al_2O_3 surface at various pH values has been reported elsewhere.[2,8] Using the information drawn from such isotherms and following the EDF methodology, two Mo/γ-Al_2O_3 samples with almost the same Mo loading (11% w/w MoO_3) were prepared using suitably selected pairs of values for the Mo concentration and pH of the impregnating solutions. The selection of the above-mentioned pairs of values will be explained in the section "Results and Discussion". Details for the method of preparation of the molybdena-supported γ-Al_2O_3 samples using EDF and the subsequent deposition of the Co-$(H_2O)_6^{2+}$ species on them by dry impregnation has been also reported recently.[6] The so prepared CoMo/γ-Al_2O_3 catalysts contained 3%w/w CoO. It should be noted that each step of the above-mentioned depositions was followed by drying at 120 °C for 2 h and then air calcination at 500 °C for 5 h.

The unpromoted and Co-promoted samples prepared are denoted as Mo_x and $CoMo_x$, respectively. We symbolize by x the pH of impregnating solution used for the deposition of the Mo-oxo species in the corresponding step.

Characterization of the Specimens. The unpromoted and promoted samples prepared for the present study were characterized using various physicochemical techniques: (i) N_2 adsorption (BET) for determining the specific surface area (SSA); (ii) diffuse reflectance spectroscopy (DRS) and laser Raman spectroscopy (LRS) for investigating the symmetry and the valence of the supported molybdenum and cobalt species; (iii) NO chemisorption for estimating the concentration of the sulfur vacancies (dynamic technique); and (iv) temperature-programmed reduction (TPR) for investigating the supported species and the active phase−carrier interactions. Experimental details for these techniques are reported in the literature.[9]

Catalytic Activity Measurements. The hydrodesulfurization (hds) activities of the unpromoted and promoted catalysts were determined in a continuous flow tubular fixed bed microreactor operating in a differential mode at atmospheric pressure. The hds of the thiophene was used as a model reaction. Full details concerning the catalytic tests and the measurements of the rates of the hds at various temperatures have been reported elsewhere.[10]

Results and Discussion

Unpromoted Catalysts: The Deposition of the Mo-Oxo Species on the γ-Al_2O_3 Surface. The adsorption isotherms achieved at pH equal to 6.3 and 3.9 are illustrated in Figure 1. It may be seen that the extent of adsorption of the Mo-oxo species is considerably higher at pH = 3.9 compared to that achieved at pH = 6.3. However, it may be observed that one may deposit almost the same amount of the Mo(VI) on the support surface using two different Mo solutions, one with $C_{eq} = 1.1 \times 10^{-3}$ mol L^{-1} and pH = 3.9 and another one with $C_{eq} = 2.7 \times 10^{-2}$ mol L^{-1} and pH = 6.3. In fact, using these solutions we have prepared through EDF two samples with the Mo content equal, respectively, to 10.5 and 11.5% w/w MoO_3. These samples are, respectively, denoted as $Mo_{3.9}$ and $Mo_{6.3}$. Although the Mo content is almost the same for these samples, it is expected that the Mo-oxo species deposited in each case differ considerably. To predict the main Mo-oxo species deposited in each case we may follow two routes.

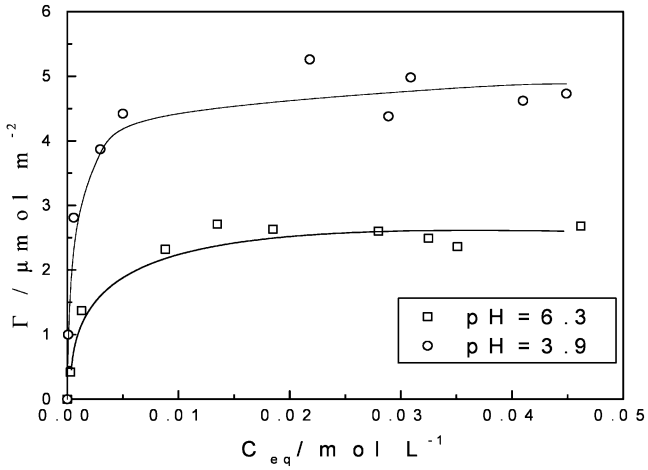

Figure 1. Experimental Mo adsorption isotherms for the pH 6.3 and 3.9. Γ: surface concentration of the deposited Mo; C_{eq}: Mo concentration of the impregnating suspension at equilibrium.

The first route is supported on the simplified one site/2pK homogeneous model[11−14] for the support surface and on the triple layer model[15,16] for the electrical double layer developed between the surface of the support particles and the impregnating solution. The application of a calculating procedure, developed by our group in the past, for the Mo deposition on the γ-Al_2O_3 surface,[1,17] which is supported on the above-mentioned models and takes into account the equilibria of the Mo-oxo species in the Mo impregnating solution, allowed us to confirm that in the alumina used in the present study the following deposition mechanism takes place:

$$AlOH_2^+ + MoO_4^{2-} \leftrightarrow AlOH_2^+ \cdots MoO_4^{2-} \quad (1)$$

$$AlOH_2^+ + Mo_7O_{24}^{6-} \leftrightarrow AlOH_2^+ \cdots Mo_7O_{24}^{6-} \quad (2)$$

$$2AlOH + MoO_4^{2-} \leftrightarrow AlOMoO_2OAl + 2OH^- \quad (3)$$

$$AlOH + MoO_4^{2-} \leftrightarrow AlOMoO_3^- + OH^- \quad (4)$$

According to this model the Mo is deposited on the support surface through adsorption of the monomeric or the polymeric Mo-oxo species on the protonated surface hydroxyls (eqs 1 and 2) and/or by surface reaction of the monomeric Mo-oxo species with the neutral surface hydroxyls (eqs 3 and 4). Moreover, the application of the above-mentioned procedure in the present study allowed us to "calculate" the deposition isotherms for each of the species illustrated in the right-hand side (rhs) of the above equilibria. These isotherms are illustrated in Figures 2 and 3, together with the corresponding calculated and experimental values for the total Mo deposition.

TABLE 1: Surface Concentration (μmol Mo/m^2) for Each of the Mo-Oxo Species Illustrated in the rhs of Equilibria 1−4

pH	$AlOH_2^+ \cdots Mo_7O_{24}^{6-}$ (μmol Mo/m^2)	$AlOH_2^+ \cdots MoO_4^{2-}$ (μmol Mo/m^2)	$AlMoO_4^-$ (μmol Mo/m^2)	Al_2MoO_4 (μmol Mo/m^2)
3.9	3.42		0.41	0.04
6.3		0.32	0.83	1.47

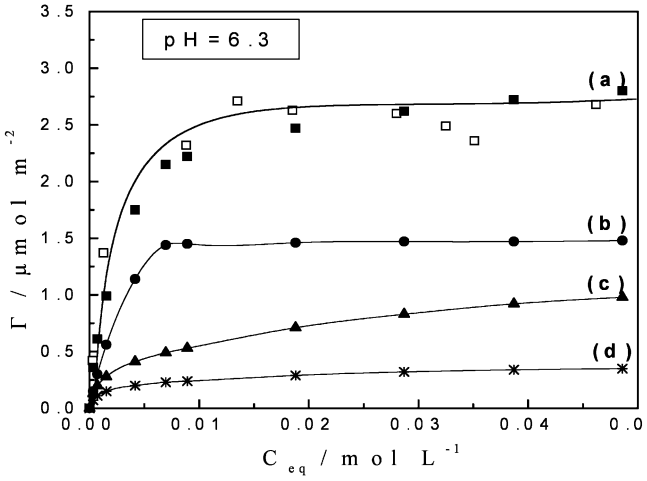

Figure 2. Mechanism of the deposition of the Mo-oxo species at pH 6.3. (a) Deposition of the total Mo-oxo species (experimental (□) and the calculated (■) values). (b) Deposition of the monomeric species through eq 3. (c) Deposition of the monomeric species through eq 4. (d) Deposition of the monomeric species through eq 1. Γ: surface concentration of the deposited Mo; C_{eq}: Mo concentration of the impregnating suspension at equilibrium.

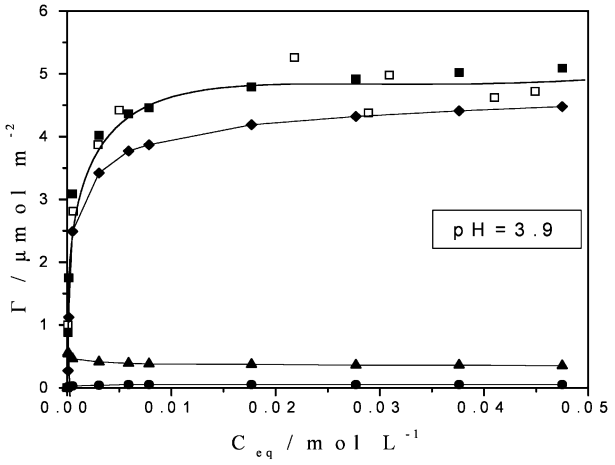

Figure 3. Mechanism of the deposition of the Mo-oxo species at pH 3.9. (a) Deposition of the total Mo-oxo species (experimental (□) and the calculated (■) values). (b) Deposition of the polymeric species through eq 2. (c) Deposition of the monomeric species through eq 4. (d) Deposition of the monomeric species through eq 3. Γ: surface concentration of the deposited Mo; C_{eq}: Mo concentration of the impregnating suspension at equilibrium.

At this point it should be stressed that, concerning the total Mo deposition isotherms (Figure 1 and Figures 2 and 3), the open symbols represent the experimental values whereas the solid symbols and the lines have been derived by "adding" the model deposition isotherms of each of the model equilibria (eqs 1−4). Moreover, the application of the above-mentioned procedure allowed us to calculate the surface concentration for each of the Mo surface species of the equilibria (eqs 1−4) under the experimental conditions used for the preparation of the catalysts $Mo_{3.9}$ and $Mo_{6.3}$ (Table 1). Inspection of Figures 2 and 3 and of Table 1 clearly shows that the Mo deposition in the catalyst $Mo_{3.9}$ proceeds principally by adsorption of the

TABLE 2: Total Surface Concentration (M) of the Positive, Neutral, and Negative Surface Hydroxyl Groups in the Impregnation Suspension

pH	$[AlOH_2^+]$/M	[AlOH]/M	$[AlO^-]$/M
3.9	1.63×10^{-3}	4.80×10^{-3}	1.78×10^{-6}
6.3	2.30×10^{-4}	4.86×10^{-3}	3.98×10^{-6}

TABLE 3: Concentration of the Mo-Oxo Species in the Impregnation Solutions

total concentration/ M	pH	MoO_4^{2-}/ M	$Mo_7O_{24}^{6-}$/ M[a]
0.0011	3.9	1.937×10^{-4}	9.07×10^{-4}
0.027	6.3	2.699×10^{-2}	6.562×10^{-6}

[a] The values refer to the moles of molybdenum.

$Mo_7O_{24}^{6-}$ species, where Mo is in octahedral symmetry, on the protonated surface hydroxyls. In contrast to that, in the catalyst $Mo_{6.3}$ the Mo deposition occurs through adsorption or reaction of the monomeric Mo-oxo species, where Mo is in tetrahedral symmetry, on the protonated or with the neutral surface hydroxyls, respectively. The above results are rather predictable for three reasons: first, because the $Mo_7O_{24}^{6-}$ species contains an amount of Mo seven times greater than that contained in the monomeric MoO_4^{2-} species; second, because the decrease in pH brings about an increase in the concentration of the protonated surface hydroxyls through the equilibria related with the one site/2p*K* model,

$$AlOH_2^+ \leftrightarrow AlOH + H^+ \quad (5)$$

$$AlOH \leftrightarrow AlO^- + H^+ \quad (6)$$

and third, because the decrease in the pH causes an increase in the polymeric Mo-oxo species in the impregnating Mo solution

$$7MoO_4^{2-} + 8H^+ \leftrightarrow Mo_7O_{24}^{6-} + 4H_2O \quad (7)$$

Using the above-mentioned calculating procedure we have calculated the surface concentration of the γ-Al_2O_3 surface groups under the experimental conditions of the catalysts preparation. The values of these surface concentrations are illustrated in Table 2. Moreover, we have calculated the concentration of the Mo-oxo species in the impregnation solution under the catalysts preparation conditions. These are illustrated in Table 3. Inspection of Tables 2 and 3 provides a reasonable explanation for the Mo surface speciation achieved, which is illustrated in the Figures 2 and 3 and Table 1. In conclusion, the use of the aforementioned calculating procedure shows that the Mo deposition in the sample $Mo_{3.9}$ takes mainly place through adsorption of the $Mo_7O_{24}^{6-}$ species on the $AlOH_2^+$ groups, whereas the Mo deposition in the sample $Mo_{6.3}$ occurs through adsorption of the MoO_4^{2-} species on the $AlOH_2^+$ groups or reaction with the AlOH groups.

In this point one might be argue that although the calculation procedure mentioned above resulted to quantitative predictions with respect to the Mo-oxo species deposited on the γ-Al_2O_3 surface in each catalyst, this calculation is supported to the approximate one site/2p*K* model (equilibria 5 and 6) and not to

the more realistic multisite model which is illustrated by the following equilibria:[18−25]

$$(Al_{oh}OH)^{-0.5} + H^+ \leftrightarrow (Al_{oh}OH_2)^{+0.5} \quad (8)$$

$$(Al_{oh}OAl_{td})^{-0.75} + H^+ \leftrightarrow (Al_{oh}OHAl_{td})^{+0.25} \quad (9)$$

$$(Al_{td}OH)^{-0.25} + H^+ \leftrightarrow (Al_{td}OH_2)^{+0.75} \quad (10)$$

$$((Al_{oh})_3O)^{-0.5} + H^+ \leftrightarrow ((Al_{oh})_3OH)^{+0.5} \quad (11)$$

$$((Al_{oh})_2OH) + H^+ \leftrightarrow ((Al_{oh})_2OH_2)^{+1} \quad (12)$$

In the above equilibria, between the surface groups of γ-Al_2O_3 developed in aqueous suspensions by Al_{oh} and Al_{td}, we symbolize surface Al^{3+} ions in octahedral and tetrahedral symmetry, respectively, whereas the numbers in the exponents represent the excess charge of the surface oxygen, assuming the ionic model for the γ-Al_2O_3. Unfortunately, the state of the art concerning the γ-Al_2O_3/aqueous solution interface does not allow one to predict the relative amounts of the Mo-oxo species deposited on the γ-Al_2O_3 surface under a given set of impregnation parameters (C_{eq} and pH). Therefore, we followed a rather qualitative approach. Inspection of the above equilibria shows that at the pH = 3.9, where the sample $Mo_{3.9}$ has been prepared, the surface groups illustrated in the right-hand sides of these equilibria should predominate. On the other hand, inspection of Table 3 shows that at this pH the $Mo_7O_{24}^{6-}$ species predominate. Taking into account the size and the charge of these polymeric ions, it seems to us reasonable to assume that at this pH the Mo deposition takes place principally by adsorption of the $Mo_7O_{24}^{6-}$ ions on one or more of the positively charged surface groups. This prediction is in agreement with recent quantitative results concerning the Mo deposition on the anatase surface.[26]

The situation is probably more complicated at pH = 6.3, where the monomeric MoO_4^{2-} ions predominate in the impregnation solution (see Table 3). Taking into account the relatively small magnitude of these ions, the above-mentioned results concerning the deposition of these ions on the γ-Al_2O_3 surface studied on the basis of the one site/2p*K* model and the recent results based on the multisite model, concerning the deposition of the MoO_4^{2-} ions on the anatase surface, we may attempt some predictions concerning the Mo deposition at pH = 6.3. By the analogy to the results drawn from the Mo deposition on the anatase surface we may speculate that the negatively charged MoO_4^{2-} ions approach the positively charged surface groups and then react with certain groups. Two factors favor the surface reactions: (i) the quite easy removal of the leaving group (water is removed more easily than the hydroxyl ions), and (ii) the shift of the excess charge of the surface oxygens to the zero, which is considered as the most stable form.[27]

Taking into account the above, it seems to us reasonable to assume that the deposition of the MoO_4^{2-} ions takes place by reaction of these ions with a single or two adjacent surface groups illustrated in the right-hand side of the equilibrium (8). This mode of deposition is described by equilibria (13) and (14).

The reactions of the MoO_4^{2-} ions with the groups illustrated in the right-hand sides of equilibria 10 and 12 seem to be rather less probable because these are related with a decrease of the excess surface charge of oxygen from +0.75 to +0.25 and from +1 to +0.5, respectively, though in both cases water molecules are released. Much less probable seem to be the reactions of the MoO_4^{2-} ions with the surface groups illustrated in the right-hand sides of equilibria 9 and 11 because in these cases the excess charge of the surface oxygens increases from +0.25 to +0.75 and from +0.5 to +1, respectively, whereas in both cases OH^- ions should be released.

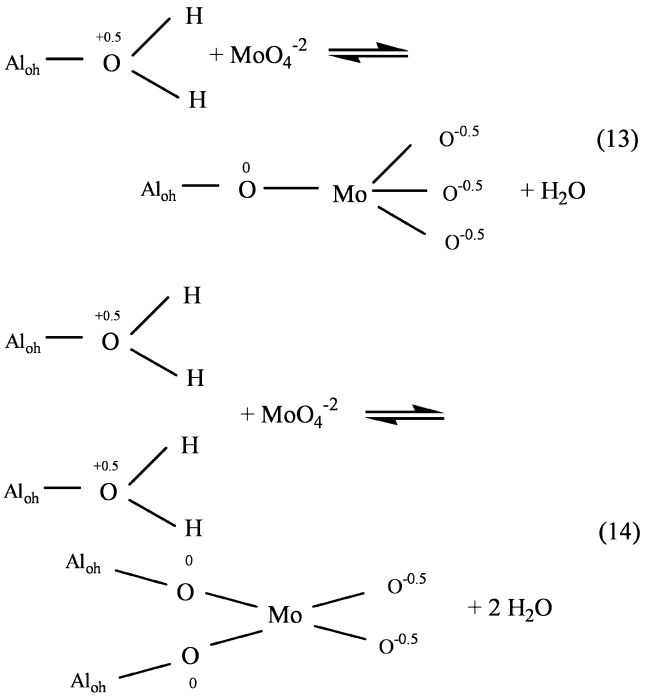

From the above considerations based on both the one site/2p*K* and the multisite/1p*K* models for the γ-Al_2O_3 surface it may be anticipated that in the $Mo_{3.9}$ sample the Mo deposition occurs mainly via the adsorption of the $Mo_7O_{24}^{6-}$ species on the protonated surface hydroxyls, whereas in the sample $Mo_{6.3}$ the Mo deposition takes place mainly via reactions of the MoO_4^{2-} ions with the neutral surface groups (homogeneous model) or with the protonated surface groups (heterogeneous model). Although the surface Mo-oxo species predicted by the homogeneous model are not identical with those predicted using the heterogeneous model, both models suggest that in the sample $Mo_{3.9}$ the deposited $Mo^{(vi)}$ is mainly in octahedral symmetry whereas in the sample $Mo_{6.3}$ it is mainly in tetrahedral symmetry.

The above predictions do not change if we take into account that at pH = 3.9 a part of the γ-Al_2O_3 surface is diluted and the Al species are moved to the solution to form a Mo−Al complex $[(Al(OH)_6Mo_6O_{18})^{3-}$ according to ref 5]. Although the formation of the afore-mentioned complex has not been observed in other similar studies [e.g., ref 28], one may consider that this complex, in which Mo is in octahedral symmetry, is mainly deposited on the γ-Al_2O_3 instead of the $Mo_7O_{24}^{6-}$ species.

Unpromoted Catalysts: Characterization. *Specific Surface Area.* Table 4 compiles the values of the specific surface area (SSA) determined for the unpromoted catalysts prepared. Inspection of Table 4 clearly shows that the SSA is not changed considerably due to the Mo deposition. This is rather expectable because in both cases EDF is used for this deposition.[6]

Diffuse Reflectance Spectroscopy. Figures 4a and 4b illustrate the DR spectra for the $Mo_{6.3}$ and the $Mo_{3.9}$ samples, respectively. Both spectra appear as a wide band in the range 400−200 nm. This band is deconvoluted into two peaks. The first one, centered at about 244 nm is attributed to the tetrahedral Mo and the second peak, centered at about 305 nm, is attributed to the octahedral Mo.[29−33] Therefore, the above spectra show that in the Mo_x samples both Mo tetrahedral and Mo octahedral species

TABLE 4: Values of the Specific Surface Area (SSA) of the Unpromoted Catalysts

catalyst	SSA/$m^2\ g^{-1}$ catalyst	SSA/$m^2\ g^{-1}\ Al_2O_3$
$Mo_{6.3}$	233	264
$Mo_{3.9}$	236	267
γ-Al_2O_3	267	267

are present. The relative magnitude of these peaks in a given sample cannot be used for estimating the relative amount of the octahedral to the tetrahedral supported Mo in that sample, due to the different values of the Mo absorption coefficient at 244 and 305 nm. However, one may use the $F(R)_{305}/F(R)_{244}$ ratio obtained in the samples to investigate the influence of the deposition conditions in the symmetry of the supported Mo. In fact, based on the values obtained for the aforementioned ratio, it may be inferred that in the $Mo_{6.3}$ sample the formation of the tetrahedral Mo is favored compared to that in the sample $Mo_{3.9}$. This is in general agreement with the trend predicted on the base of the deposition models. In this point it should be stressed that the prediction mentioned above is not quantitative because in the subsequent preparation steps, mainly during the air calcination, the Mo supported species are considerably changed. This should be also taken into account considering the physicochemical characterization results achieved using the remainder techniques.

Laser Raman Spectroscopy. Figure 5 illustrates the L. R. spectra recorded for the unpromoted catalysts prepared. According to the literature the monomeric tetrahedral Mo-oxo species appear LR bands at about 320 and 940 cm^{-1}, whereas the polymeric octahedral Mo-oxo species appear LR bands at about 360 and 970 cm^{-1}.[30,33−37] Moreover, a band appeared at 220 cm^{-1} indicates the presence of polymeric species.

In both spectra appeared bands at 220 cm^{-1} and in the range 300−400 and 700−1000 cm^{-1}. The above bands indicate the presence of rather well dispersed Mo-oxo species on the support surface. Moreover, the absence of an intense and sharp peak at 820 cm^{-1} indicates no formation of supported MoO_3 crystallites.[38] It may be observed that the peaks appeared at about 970 cm^{-1} and 220 cm^{-1} are more intense in the $Mo_{3.9}$ than in the $Mo_{6.3}$ sample. This strongly suggests that in this sample the formation of the octahedral supported Mo is favored, in agreement with the DRS results. To investigate further this point we have deconvoluted the bands appeared in the range 600−1000 cm^{-1}. The result of this deconvolution is illustrated in the Figures 6a and 6b. Moreover, we have calculated the area under the peaks centered at about 220, 940 and 960 cm^{-1}. Table 5 compiles the values of these areas. These values suggest that the formation of the octahedral supported Mo is favored in the sample $Mo_{3.9}$, as it is compared to that formation in the sample $Mo_{6.3}$.

Temperature-Programmed Reduction (TPR). The TPR curves for the Mo_x specimens studied are illustrated in Figure 7. Two peaks appear at about 500 and 900 °C. These are typical of the well-dispersed molybdenum supported species.[39−49] On the other hand, the absence of an additional reduction peak at about 600 °C indicates no formation of bulk MoO_3 on the support surface.[43] However, the interpretation of the reduction profiles of the Mo_x samples is not straightforward. In earlier works the reduction peaks are generally associated with the complete reduction of a particular species at a given temperature range.[39−42] More specifically, the peak centered at about 500 °C was attributed to the loosely bonded supported Mo, whereas the peak centered at about 900 °C was attributed to the supported Mo phase strongly interacted with the support surface. In contrast to the above, on the basis of recent works,[44−49] it may

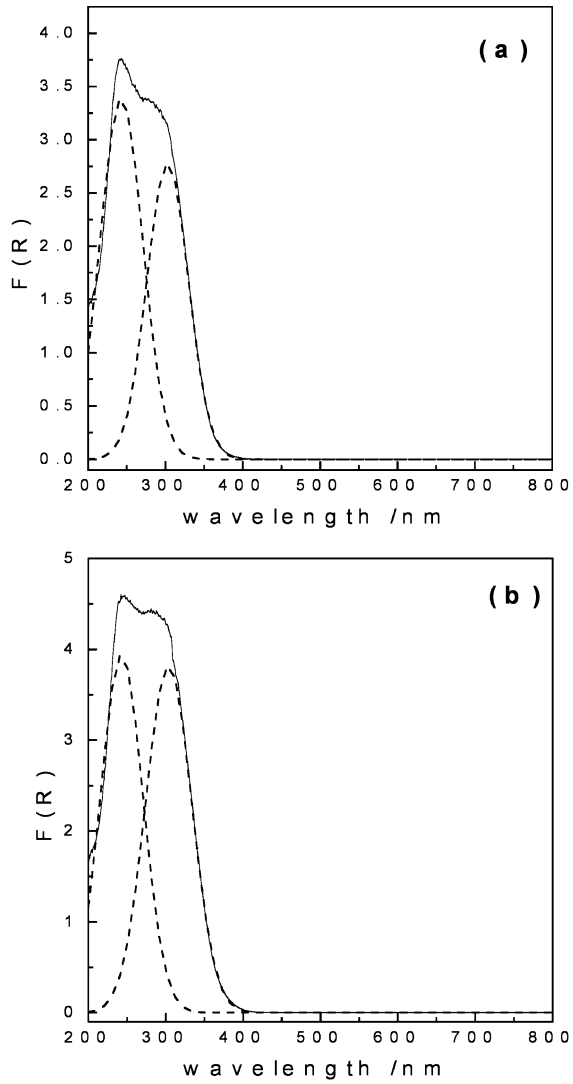

Figure 4. DR spectra recorded in the range 200−800 nm for the $Mo_{6.3}$ (a) and for the $Mo_{3.9}$ (b) catalyst.

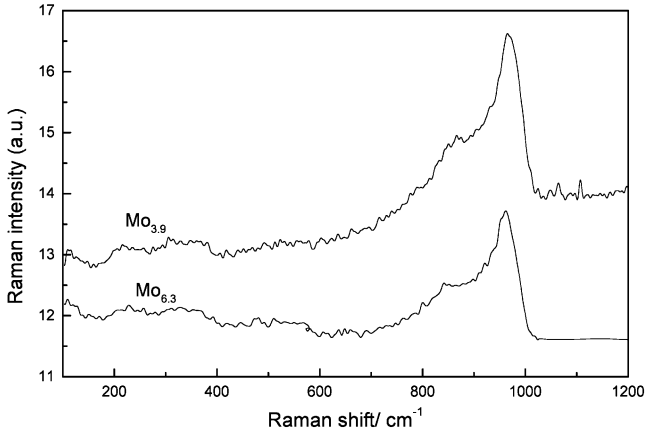

Figure 5. LR spectra recorded in the range 150−1200 cm^{-1} for the unpromoted catalysts.

be inferred that the reduction of at least some supported Mo-oxo species takes place in two steps: Mo(VI) to Mo(IV) and then Mo(IV) to Mo(metal). Following this stepwise Mo reduction, the low-temperature reduction peak is attributed to the first step whereas the high-temperature reduction peak is attributed to the second step.

To investigate whether the stepwise reduction in our cases is related to the total supported Mo phase we have calculated

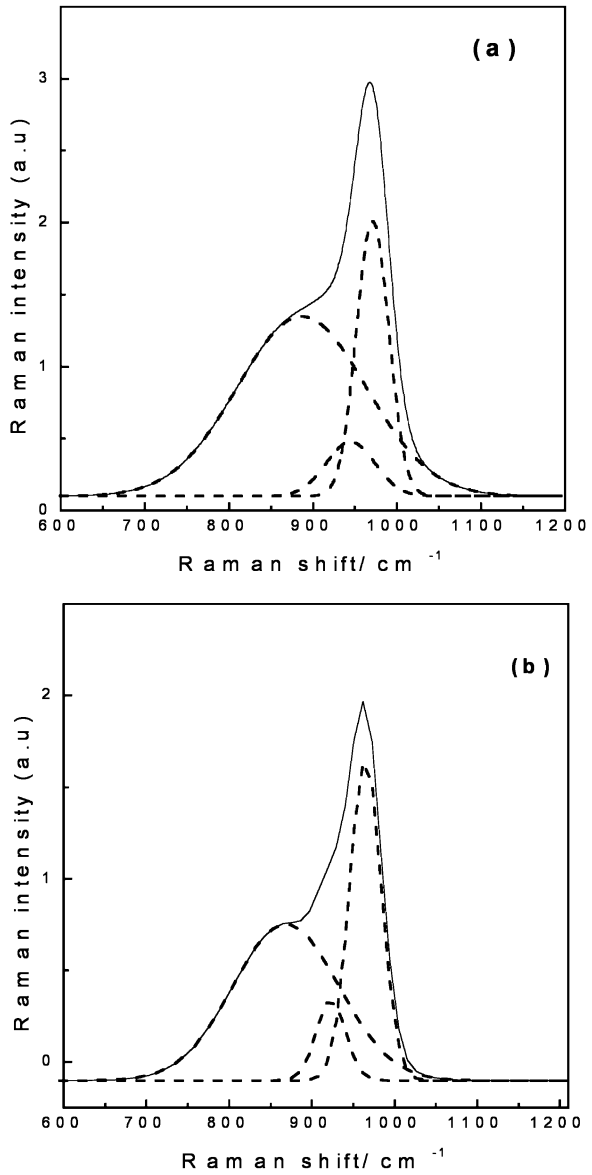

Figure 6. Deconvolution of the LR spectra in the range 600−1100 cm^{-1} for the $Mo_{6.3}$ (a) and for the $Mo_{3.9}$ (b) catalyst.

TABLE 5: Calculated Area (a.u.) under Each Peak Centered at 220, 940, and 960 cm^{-1} for the Unpromoted Catalysts

catalyst	area of peak in 940 cm^{-1}	area of peak in 960 cm^{-1}	area of peak in 220 cm^{-1}
$Mo_{6.3}$	35.542	55.678	10.1
$Mo_{3.9}$	35.117	84.341	14.9

separately the area under the low- and the high-temperature reduction peak as well as the degree of the Mo reduction for the total supported Mo (mol of H_2 consumed/mol of H_2 required for the total reduction of the Mo species: Mo(VI) to Mo(metal)) The results are compiled in Table 6. It may be observed that for both samples the degree of the Mo reduction is lower than unity, which means that some supported Mo-oxo species are not completely reduced even at 1000 °C. Moreover, it may be observed that in the $Mo_{6.3}$ sample the ratio of the areas (*S*) mentioned above, *S*(peak at 930 °C)/*S*(peak at 545 °C), is greater than 2, whereas for the sample $Mo_{3.9}$ this ratio, *S*(peak at 910 °C)/*S*(peak at 540 °C), is lower than 2. The above suggest that on the γ-Al_2O_3 surface are formed more than one Mo-oxo species with different reducibility. Moreover, these indicate that

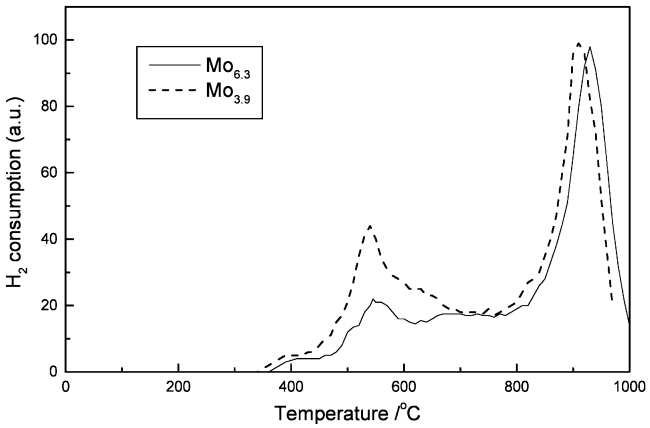

Figure 7. Temperature-programmed reduction curves for the unpromoted catalysts.

TABLE 6: Temperatures of the TPR Peaks Maxima, Ratios of the TPR Peaks Area, *S*(peak at high temperaure)/[*S*(peak at low temperaure)], and the Degree of Reduction (see text) for the Unpromoted Catalysts

catalyst	1st peak/ °C	2nd peak/ °C	*S*(peak at high temperaure)/ [*S*(peak at low temperaure)]	degree of reduction
$Mo_{6.3}$	545	930	2.86	0.553
$Mo_{3.9}$	540	910	1.64	0.723

the composition of the supported phase is different in the two Mo_x samples. Specifically, in the $Mo_{6.3}$ sample the peak at 930 °C should be responsible not only for the Mo(IV) to the Mo (metal) reduction step of the Mo-oxo species whose reduction had been started at 545 °C but, in addition, for the reduction (rather incomplete) of the Mo-oxo species not reducible at the lower temperature. It seems to us plausible to assume that these species are strongly interacted with the support surface. In contrast to the above, in the $Mo_{3.9}$ sample the peak at 540 °C should be not only responsible for the first reduction step (Mo(VI) to Mo(IV)), but also attributed to the more reducible Mo supported species whose reduction proceeds further than the Mo(IV) at 540 °C. It seems to us plausible to assume that these Mo-oxo species are loosely bonded with the support surface—probably polymeric Mo-oxo species deposited on the support surface by adsorption of the polymeric Mo-oxo species (see for example eq 2). In this point one might be argue that the lower than 2 value determined for the $Mo_{3.9}$ (see Table 6) could be attributed to the fact that a portion of the partially reduced Mo species at 540 °C does not continue its reduction at 910 °C. We are inclined to believe that this is not the case for two reasons: first, because the $Mo_{3.9}$ sample exhibited higher total reducibility than that exhibited by the sample $Mo_{6.3}$ (see Table 6); and second ,because the high temperature reduction peaks observed in both samples have practically the same magnitude. Finally, a shift of the second reduction peak to lower temperature going from the $Mo_{6.3}$ to the $Mo_{3.9}$ sample may be seen. This indicates that even the high temperature reducible Mo is more easily reducible in the $Mo_{3.9}$ than in the $Mo_{6.3}$ sample.

In this point it should be noticed that as the reduction through sulfidation of the Mo(VI) to Mo(IV) takes place at 400 °C, one may assume that the low temperature reduction peak (and the loosely bonded supported Mo species) is more relevant to the sulfided active phase formed.

In conclusion, the TPR curves show that in the sample $Mo_{3.9}$ larger amounts of loosely bound and more easily reducible Mo-oxo species are formed than those formed in the $Mo_{6.3}$ sample.

TABLE 7: Values of the Chemisorbed NO over the Unpromoted Catalysts

catalyst	chemisorbed NO/ μmol g^{-1}
$Mo_{6.3}$	58.0
$Mo_{3.9}$	68.3

Concentration of Sulfur Vacancies. It is accepted that the NO chemisorbed per gram of the sulfided Mo/γ-Al_2O_3 catalysts may be used to estimate the concentration of the sulfur vacancies considered to be responsible for the acceleration of the hydrodesulfurization reactions.[50,51] Table 7 compiles the amount of the chemisorbed NO over the catalysts studied. It may be observed that the $Mo_{3.9}$ exhibits a sulfur vacancies concentration which is higher than that exhibited by the $Mo_{6.3}$ sample. A plausible explanation is that the relatively loosely bound and easily reducible Mo polymeric (or complexed with Al) supported phase in the $Mo_{3.9}$ sample is more easily sulfided as it is compared to the Mo supported phase in the $Mo_{6.3}$ sample. Thus, the more supported Mo there is in the sulfided state, the higher the concentration of the sulfur vacancies related with the active sites.

Predictions of the Deposition Models and the Characterization Results. Having accomplished the characterization of the supported specimens, let us now concentrate our attention on the predictions presented in the section "Unpromoted Catalysts: The Deposition of the Mo-Oxo Species on the γ- Al_2O_3 Surface" in light of the characterization results. First it should be noted again that during drying and calcination, which follows deposition, the deposited Mo phase is somewhat reconstructed. Therefore, one cannot expect that the Mo speciation achieved on the support surface after deposition would be identical to that obtained after calcination.[7,29,52] Thus, the question is whether the transformations taking place during drying and calcination render, from the viewpoint of catalysis, of no interest the Mo surface speciation achieved after Mo deposition. Different answers have been reported so far to the above-mentioned question. According to the first answer, the final speciation of the Mo phase is mainly determined from the nature (point of zero charge) of the support and the Mo loading and not from the preparation technique and the critical preparation parameters, such as the impregnation pH. This answer is supported on the assumption that, irrespectively of the preparation method followed for the Mo deposition, during drying the hydrated catalyst surfaces behave as if they are in a aqueous environment and the molybdate speciates at the pH of the hydrous surface layer which is solely a function of the weighted average of the pzcs of the MoO_3 and γ- Al_2O_3.[34,53−56] This assumption interprets quite well the influence of the pzc on the Mo-oxo species formed on the surface of a series of supports (SiO_2, γ- Al_2O_3, TiO_2, ...). However, results obtained by Hu et al.[57] on Nb_2O_5-supported catalysts could not be explained within the pzc model.

Despite the above, extensive studies performed by our group concerning the influence of the preparation of the Mo/γ-Al_2O_3 and W/γ-Al_2O_3 catalysts have shown that the preparation method followed for depositing the Mo (or W) species influences considerably the structure and the reactivity of the oxidic supported phase as well as the sulfided phase and the catalytic activity.[6,58−60] The present characterization results show that even in the case where the same methodology is applied for depositing the Mo-oxo species, the different speciation achieved after the Mo deposition at the two different pHs causes the formation of somewhat different structures concerning the Mo oxidic and the final sulfided state. The above are in agreement with the results obtained by other authors who applied the EDF preparation technique.[7,29] A plausible explanation is that following EDF *from very diluted Mo solutions*, the deposition of almost all the Mo-oxo species takes place in the impregnation step (during the long time equilibration of the suspension) and not during the subsequent step of drying. However, during drying and mainly calcination and sulfidation, the relatively high temperature of heating brings about transformations in the Mo supported phase, which however, cannot neutralize completely the influence of the initial surface Mo speciation on the final structure of the supported Mo phase.

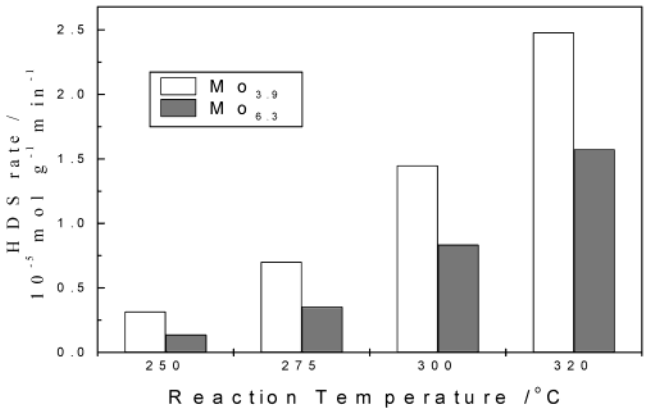

Figure 8. Rate of hydrodesulfurization of thiophene achieved over the unpromoted catalysts.

TABLE 8: Values of the Specific Surface Area (SSA) for the Promoted Catalysts

catalyst	SSA/ $m^2\,g^{-1}$ catalyst	SSA/ $m^2\,g^{-1}$ Al_2O_3
$CoMo_{6.3}$	201	232
$CoMo_{3.9}$	191	223
γ-Al_2O_3	267	267

Catalytic Activity. Figure 8 illustrates the hydrodesulfurization activity achieved for the unpromoted catalysts prepared. It may be seen that at all temperatures studied the hydrodesulfurization rate is higher for the sample $Mo_{3.9}$ compared to that achieved for the $Mo_{6.3}$ sample.

In view of the DRS, LRS, TPR, and NO chemisorption results, this catalytic behavior is rather predictable. In fact, the Mo deposition at relatively low pH (pH = 3.9) favors the deposition of the polymeric (or complexed with Al) Mo phase loosely bound with the support surface and easily reducible. This phase is related with a relatively high concentration of the sulfur vacancies in the sulfided state and, thus, with a relatively high hydrodesulfurization activity. The plausible question in this point is whether the influence of the deposition pH stated above could be also observed in the Co promoted catalysts. The results and discussion followed will be devoted to the investigation of this point.

Promoted Catalysts. *The Deposition of the Co^{2+} Species on the Mo_x Samples.* As already mentioned, the Co deposition on the promoted Mo_x samples was carried out by dry impregnation. In both cases an amount of cobalt equal to 3% w/w CoO has been mounted on the surface of the Mo_x samples.

Specific Surface Area. Table 8 compiles the values of the specific surface area (SSA) determined for the promoted catalysts prepared. Inspection of Table 8 clearly shows that the SSA is not considerably different in the two promoted samples. It is may also be seen that Co deposition decreases slightly the SSA of the samples.

Diffuse Reflectance Spectroscopy. Figure 9 illustrates the DR spectra for the Co-promoted $Mo_{3.9}$ and $Mo_{6.3}$ catalysts denoted

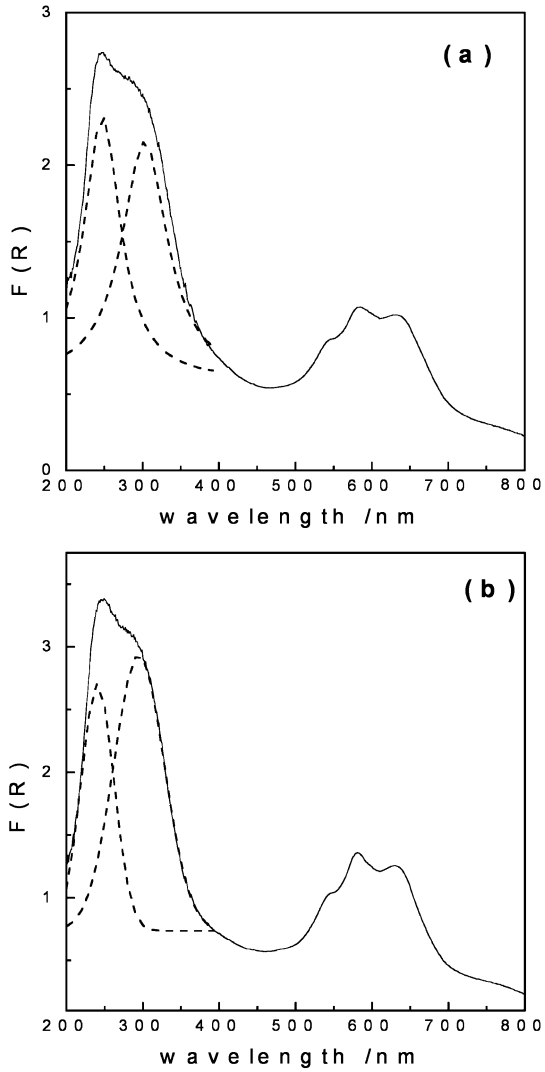

Figure 9. DR spectra recorded in the range 200−800 nm for the $CoMo_{6.3}$ (a) and for the $CoMo_{3.9}$ (b) catalyst.

TABLE 9: Values of the Ratio of the K-M Function Determined at 425 and 600 nm, $F(R)_{425}/[F(R)_{425} + F(R)_{600}]$

catalyst	$F(R)_{425}/[F(R)_{425} + F(R)_{600}]$
$CoMo_{6.3}$	0.33
$CoMo_{3.9}$	0.38

by $CoMo_{3.9}$ and $CoMo_{6.3}$, respectively. Both spectra exhibit the wide band in the range 400−200 nm which is related with the presence of the supported Mo. Inspection of this band shows that, as in the case of the unpromoted samples, the deposition of Mo at pH = 3.9 favors deposition of the polymeric (or complexed with Al) octahedral Mo phase. To better investigate this point we have deconvoluted the band in the range 400−200 nm in two peaks, as in the case of the unpromoted catalysts. The deconvolution results achieved show that this is, in fact, the case.

Moreover, in the spectra of Figure 9 a triplet band appears centered at about 600 nm, which is characteristic of the tetrahedral Co as well as a wide band centered at about 425 nm which is attributed to the octahedral Co.[61−63] To investigate the influence of the pH at which the Mo deposition takes place on the symmetry of the supported Co, we have calculated the ratio $F(R)_{425}/(F(R)_{425} + F(R)_{600})$. Inspection of Table 9 shows that in the $CoMo_{3.9}$ catalyst the above-mentioned ratio is higher than that determined for the $CoMo_{6.3}$ catalyst. A plausible explanation is that in the $Mo_{3.9}$ sample the well-dispersed Mo polymeric species better hinders the deposition of the Co^{2+} species on the γ-Al_2O_3 surface and thus the formation of the catalytically inactive $CoAl_2O_4$, in which Co is in tetrahedral symmetry.

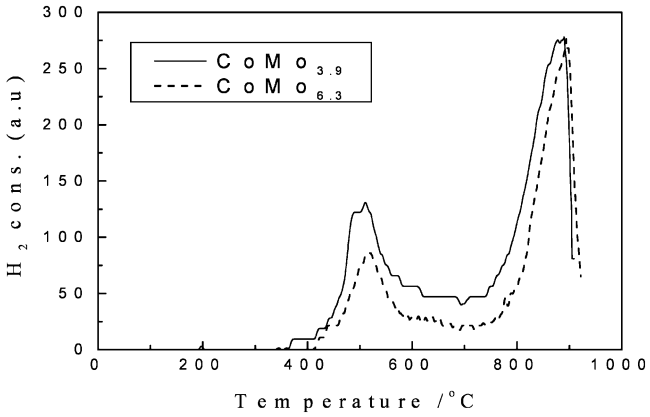

Figure 10. Temperature-programmed reduction curves for the Co-promoted catalysts.

TABLE 10: Temperatures of the TPR Peaks Maxima, Ratios of the TPR Peaks Area, *S*(peak at high temperaure)/[*S*(peak at low temperaure)], and the Degree of Reduction (see text) for the Promoted Catalysts

catalyst	1st peak/ °C	2nd peak/ °C	*S*(peak at high temperaure)/ [*S*(peak at low temperaure)]	degree of reduction
$CoMo_{6.3}$	516	897	2.48	0.31
$CoMo_{3.9}$	505	886	1.72	0.47

Temperature-Programmed Reduction. The TPR curves for the samples $CoMo_{3.9}$ and $CoMo_{6.3}$ are illustrated in Figure 10 whereas the TPR data drawn from these curves are compiled in Table 10. Comparison of the curves illustrated in Figure 10 and Table 10 with those illustrated in Figure 7 and Table 6 clearly shows that the deposition of Co does not change considerably the conclusion drawn concerning the influence of deposition pH on the reductive behavior of the supported Mo. In fact, even after Co deposition, the peak centered at about 500 °C, which as already mentioned reflects the first step of the Mo reduction (Mo(VI) to Mo(IV)) relevant to the catalysis and may be partly attributed to the loosely bound supported Mo, is greater in the $CoMo_{3.9}$ than in the $CoMo_{6.3}$ sample.

Moreover, as in the case of the unpromoted samples, a shift may be observed in the reduction peak that appears at about 900 °C to the lower temperature going from the $CoMo_{6.3}$ to the $CoMo_{3.9}$ sample. Furthermore, the area under the reduction curve of the $CoMo_{6.3}$ is smaller than that of the $CoMo_{3.9}$ sample. The above show that in the $CoMo_{3.9}$ sample larger amounts of the weakly interacted and more easily reduced Mo-oxo species are formed than those formed in the $CoMo_{6.3}$ sample.

It may be observed that the presence of the supported Co phase decreases the temperature at which the Mo reduction peaks appear and this should be related with the promotive action of this phase. The decrease in the degree of reduction, now calculated for the total supported phase (compare Table 6 with Table 10), suggests that a part of the Co^{2+} species, presumably $CoAl_2O_4$, is not reduced. The above are corroborated by the DRS results.

Finally, the absence of reduction peaks at about 350 °C clearly shows that we have no formation of cobalt oxide (Co_3O_4) and Co^{2+} strongly interacted with the surface of the γ-Al_2O_3.[63,64] This suggests that almost all the surface Co phase interacts with the supported Mo phase.

The comparative examination of the physicochemical characterization results of Mo_x with the corresponding $CoMo_x$

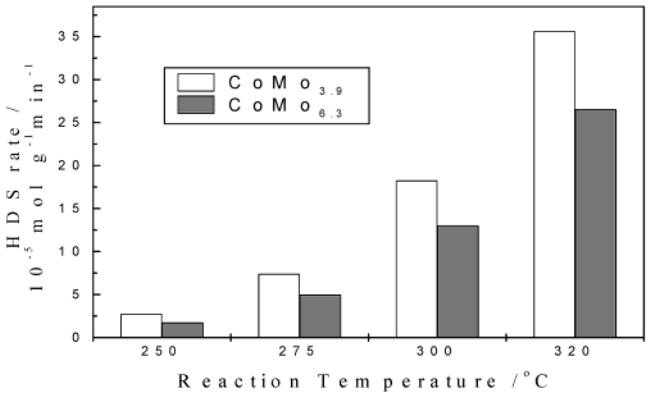

Figure 11. Rate of hydrodesulfurization of thiophene achieved over the Co-promoted catalysts.

samples showed that the Co deposition influenced some of the physicochemical characteristics of the initially formed Mo supported phase (compare for example the TPR curves). However, the above-mentioned comparative examination showed that the general trends concerning the influence of impregnating pH on the structure of the Mo supported phase are not changed due to the Co deposition.

Catalytic Activity. Figure 11 illustrates the hydrodesulfurization activity achieved for the $CoMo_{3.9}$ and $CoMo_{6.3}$ catalysts prepared. It may be observed that, in all temperatures studied, the rate of hydrodesulfurization is higher in the $CoMo_{3.9}$ than in the $CoMo_{6.3}$ catalyst.

Taking into account the DRS and TPR results drawn for the promoted catalysts as well as the characterization results concerning the unpromoted samples we may attribute the relatively high catalytic activity exhibited by the $CoMo_{3.9}$ catalyst to the fact that the deposition at a relatively low pH favors the deposition of a polymeric (or complexed with Al) Mo-oxo species. After calcination these species provide a well-dispersed supported Mo phase with relatively high reducibility. This phase hinders the formation of the catalytically inactive $CoAl_2O_4$, whereas after sulfidation provides a sulfided state with relatively high concentration in sulfur vacancies. Both effects result in a $CoMo/\gamma\text{-}Al_2O_3$ catalyst with relatively high catalytic activity.

Conclusions

The most important findings drawn from the present work may be summarized as follows.

1. The unpromoted and the Co-promoted molybdena supported $\gamma\text{-}Al_2O_3$ catalysts where the Mo deposition on the support surface, by EDF, carried out at relatively low pH and low Mo concentration in the impregnating solution were found to be more active in the hydrodesulfurization of thiophene than the corresponding catalysts prepared by depositing Mo on the support surface at a relatively high pH and high concentration of the impregnating solution.

2. In the steps of preparation, which follow the Mo deposition, the Mo supported species are changed considerably. Therefore the Mo speciation done on the base of the two models related with the acid−base behavior of the $\gamma\text{-}Al_2O_3$ surface may be used only for predicting general trends concerning the Mo species formed after the air-calcination.

3. The characterization of the unpromoted and the Co-promoted specimens showed that the Mo deposition, at relatively low pH, favors the deposition of polymeric (or complexed with Al) Mo-oxo species, in line with predictions drawn on the basis of the aforementioned models.

4. After calcination of the specimens prepared at relatively low pH, the deposited Mo-oxo species provide a well-dispersed Mo phase with relatively high reducibility. This phase, in which the concentration of the octahedral Mo is greater compared to that in the specimens where the Mo deposition carried out at relatively high pH, hinders the formation of the catalytically inactive $CoAl_2O_4$, whereas after activation it provides a sulfided state with a relatively higher concentration in sulfur vacancies.

5. The above explain the catalytic results mentioned in point 1, indicating that the selection of the proper impregnating parameters, using EDF, may be proved quite critical for the achievement of high catalytic activity.

Acknowledgment. The General Secretariat of Research and Technology, Hellas, is gratefully acknowledged for providing the financial support for this work (research project EKBAN2 # 39). We gratefully acknowledge experimental assistance by Dr. G. A. Voyiatzis in recording laser Raman spectra.

References and Notes

(1) Spanos, N.; Vordonis, L.; Kordulis, Ch.; Lycourghiotis, A. *J. Catal.* **1990**, *124*, 301.
(2) Spanos, N.; Vordonis, L.; Kordulis, Ch.; Koutsoukos, P. G.; Lycourghiotis, A. *J. Catal.* **1990**, *124*, 315.
(3) Spanos, N.; Lycourghiotis, A. *J. Catal.* **1994**, *147*, 57.
(4) Spanos, N.; Lycourghiotis, A. *Langmuir* **1994**, *10*, 2351.
(5) Carrier, X.; Lambert, J.-F.; Che, M. *J. Am. Chem. Soc.* **1997**, *119*, 10137.
(6) Papadopoulou, Ch.; Vakros, J.; Matralis, H. K.; Voyiatzis, G. A.; Kordulis, Ch.; Lycourghiotis, A. *J. Colloid Interface Sci.* **2003**, in press.
(7) Wang, L.; Hall, W. K. *J. Catal.* **1983**, *83*, 242.
(8) Vakros, J. Ph.D. Thesis, University of Patras, 1997.
(9) Georgiadou, I.; Papadopoulou, Ch.; Matralis, H. K.; Voyiatzis, G. A.; Lycourghiotis, A.; Kordulis, Ch. *J. Phys. Chem B* **1998,** *102*, 8459.
(10) Vakros, J.; Kordulis, Ch. *Appl. Catal. A* **2001**, *217*, 287.
(11) Healy, T. W.; White, L. R. *Adv. Colloid Interface* **1978**, *9*, 303.
(12) Huang, C. P.; Stumm, W. *J. Colloid Interface Sci.* **1973**, *43*, 409.
(13) Brunelle, J. P. *Pure Appl. Chem.* **1978**, *50*, 1211.
(14) Parfitt, G. D. *Pure Appl. Chem.* **1976**, *48*, 415.
(15) James, R. O.; Davis, J. A.; Leckie, J. O. *J. Colloid Interface Sci.* **1978**, *65*, 331.
(16) Davis, J. A.; Leckie, J. O. *J. Colloid Interface Sci.* **1980**, *74*, 32.
(17) Bourikas, K.; Matralis, H. K.; Kordulis, Ch.; Lycourghiotis, A. *J. Phys. Chem.* **1996**, *100*, 11711.
(18) Hiemstra, T.; Van Riemsdijk, W. H.; Bolt, G. H. *J. Colloid Interface Sci.* **1989**, *133*, 91.
(19) Hiemstra, T.; De Wit, J. C. M.; Van Riemsdijk, W. H. *J. Colloid Interface Sci.* **1989**, *133*, 105.
(20) Hiemstra, T.; Van Riemsdijk, W. H. *Colloids Surf.* **1991**, *59*, 7.
(21) Hiemstra, T.; Venema, P.; Van Riemsdijk, W. H. *J. Colloid Interface Sci.* **1996**, *184*, 680.
(22) Contescu, C.; Popa, V.; Miller, J. B.; Ko, E. I.; Schwarz, J. A. *J. Catal.* **1995**, *157*, 244.
(23) Contescu, C.; Contescu, A.; Schramm, C.; Sato, R.; Schwarz, J. A. *J. Colloid Interface Sci.* **1994**, *165*, 66.
(24) Contescu, C.; Contescu, A.; Schwarz, J. A. *J. Phys. Chem.* **1994**, *98*, 4327.
(25) Contescu, C.; Popa, V.; Schwarz, J. A. *J. Colloid Interface Sci.* **1996**, *180*, 149.
(26) Bourikas, K.; Hiemstra, T.; Van Riemsdijk, W. H. *J. Phys. Chem. B* **2001**, *105*, 2393.
(27) Bargar, J. R.; Brown, G. E., Jr.; Parks, G. A. *Geochim. Cosmochim. Acta* **1997**, *61*, 2639.
(28) Vissenberg, M. J.; Joosten, L. J. M.; Heffels, M. M. E. H.; van Welsens, A. J.; de Beer, V. H. J. (San); van Santen, R. A.; van Veen, J. A. R. *J. Phys. Chem. B* **2000**, *104*, 8456.
(29) Wang L.; Hall, W. K. *J. Catal.* **1982**, *77*, 232.
(30) Jeziorowski, H.; Knozinger, H. *J. Phys. Chem.* **1979**, *83*, 1166.
(31) Damyanova, S.; Spojakina, A.; Jiratova, K. *Appl. Catal. A:* General **1995**, *125*, 257.
(32) Henker, M.; Wendlandt, K. P.; Valyon, J.; Bornmann, P. *Appl. Catal.* **1991**, *69*, 205.
(33) Mestl, G.; Srinivasan, T. K. K. *Catal. Rev.—Sci. Eng.* **1998**, *40*, 451.
(34) Williams, C. C.; Ekerdt, J. G.; Jehng, J. M.; Hardcastle, F. D.; Wachs, I. E. *J. Phys. Chem.* **1991**, *95*, 8791.

(35) Van Veen, J. A. R.; De Wit, H.; Emeis, C. A.; Hendriks, P. A. J. M. *J. Catal*. **1987**, *107*, 579.
(36) Knozinger, H.; Jeziorowski, H. *J. Phys. Chem.* **1978**, *82*, 2002.
(37) Stencel, J. M.; Makovsky, L. E.; Sarkys, T. A.; De Vries, J.; Thomas, R.; Moulijn, J. A. *J. Catal.* **1984**, *90*, 314.
(38) Del Arco, M.; Carrazan, S. R. G.; Martin, C.; Rives, V.; Garcia-Ramos, J. V.; Carmona, P. *Spectrochim. Acta* **1994**, *50A*, 2215.
(39) Lopez Cordero, R.; Gil Llambias, F. J.; Lopez Agudo, A. *Appl. Catal*. **1991**, *74*, 125.
(40) Zhaobin, W.; Qin, X.; Xiexian, G.; Grange, P.; Delmon, B. *Appl. Catal*. **1991**, *75*, 179.
(41) Goula, M. A.; Kordulis, Ch.; Lycourghiotis, A.; Fierro, J. L. G. *J. Catal*. **1992**, *137*, 285.
(42) Brito, J.; Laine, J. *Polyhedron* **1986**, *5*, 179.
(43) Rajagopal, S.; Marini, H. J.; Marzari, J. A.; Miranda, R. *J. Catal*. **1994**, *147*, 417.
(44) Regalbuto, J. R.; Ha, J. W. *Catal. Lett.* **1994**, *29*, 189.
(45) Del Arco, M.; Carrazan, S. R. G.; Rives, V.; Llambias, F. L. G.; Malet, P. *J. Catal.* **1993**, *141*, 48.
(46) Chary, K. V. R.; Reddy, K. R.; Kumar, C. P. *Catal. Commun.* **2001**, *2*, 277.
(47) Noronha, F. B.; Baldanza, M. A. S.; Schmal, M. *J. Catal.* **1999**, *188*, 270.
(48) Abello, M. C.; Gomez, M. F.; Ferreti, O. *Appl. Catal. A* **2001**, *207*, 421.
(49) Damyanova, S.; Petrov, L.; Centero, M. A.; Grange, P. *Appl. Catal. A* **2002**, *224*, 271.
(50) Kulkarni, G. U.; Rao, C. N. R. *Catal. Lett.* **1991**, *11*, 63.
(51) Portela, L.; Grange, P.; Delmon, B. *Catal. Rev.—Sci. Eng.* **1995**, *37*, 699.
(52) Xiong, G.; Feng, Z.; Li, J.; Yang, Q.; Ying, P.; Xin, Q.; Li, C. *J. Phys. Chem. B* **2000**, *104*, 3588.
(53) Reddy, B. M.; Reddy, E. P.; Srinivas, S. T. *J. Catal.* **1992**, *136*, 50.
(54) Wachs, I. E. *Catal. Today* **1996**, *27*, 437.
(55) Williams, C. C.; Ekerdt, J. G.; Jehng, J. M.; Hardcastle, F. D.; Turek, A. M.; Wachs, I. E. *J. Phys. Chem.* **1991**, *95*, 8781.
(56) Korangi, T. I.; Paal, Z.; Leyrer, J.; Knozinger, H. *Appl. Catal.* **1990**, *64*, L5.
(57) Hu, H.; Wachs, I. E.; Bare, S. R. *J. Phys. Chem*. **1990**, *99*, 10897.
(58) Karakonstantis, L.; Bourikas, K.; Lycourghiotis, A. *J. Catal*. **1996**, *162*, 295.
(59) Karakonstantis, L.; Matralis, H.; Kordulis, Ch.; Lycourghiotis, A. *J. Catal*. **1996**, *162*, 305.
(60) Lycourghiotis, A. In *Preparation of Catalyst VI*; Ponselet, G., Martens, J., Delmon, B., Jacobs P. A., Grange, P., Eds.; Elsevier: Amsterdam, 1995; p 95.
(61) Lycourghiotis, A. In *Preparation of Catalyst III*; Ponselet, G., Grange, P., Jacobs, P. A., Eds.; Elsevier: Amsterdam, 1983; p 343.
(62) Lycourghiotis, A.; Kotinopoulos, M. *React. Solids* **1985**, *1*, 95.
(63) Vakros, J.; Kordulis, Ch.; Lycourghiotis, A. *Langmuir* **2002**, *18*, 417.
(64) Arnoldy, P.; Moulijn, J. A. *J. Catal*. **1985**, *93*, 38.